

Attention Augmented ConvLSTM for Environment Prediction

Bernard Lange, Masha Itkina, Mykel J. Kochenderfer

Stanford University

{blange, mitkina, mykel}@stanford.edu

Abstract: Safe and proactive planning in robotic systems generally requires accurate predictions of the environment. Prior work on environment prediction applied video frame prediction techniques to bird’s-eye view environment representations, such as occupancy grids. ConvLSTM-based frameworks used previously often result in significant blurring and vanishing of moving objects, thus hindering their applicability for use in safety-critical applications. In this work, we propose two extensions to the ConvLSTM to address these issues. We present the Temporal Attention Augmented ConvLSTM (TAAConvLSTM) and Self-Attention Augmented ConvLSTM (SAAConvLSTM) frameworks for spatiotemporal occupancy prediction, and demonstrate improved performance over baseline architectures on the real-world KITTI and Waymo datasets. We provide our implementation at <https://github.com/sisl/AttentionAugmentedConvLSTM>.

Keywords: Environment Prediction, Perception, Autonomous Driving, Deep Learning, Attention

1 Introduction

Environment prediction is critical for developing intelligent agents capable of safe interaction with the surroundings, such as drones and autonomous vehicles. Urban driving involves a multitude of complex scenarios that contain cluttered and obscured environments with a variety of moving and static obstacles. Experienced human drivers understand the semantics of the scene and can anticipate the future motion of other traffic participants. They implicitly use this knowledge to ensure the safety and comfort of their resulting maneuvers. Likewise, trajectory planning algorithms and decision-making frameworks must consider the inherent temporality of the perceived state and plan proactively to facilitate safe and comfortable transportation [1, 2].

Environment prediction architectures fall into two paradigms. A *classical robotics approach* involves multiple sequential stages such as object detection and classification, state estimation, and motion modeling [3–7]. However, this approach often requires full observability and operates on heavily preprocessed information. In contrast, a *neural network-based approach* uses minimally processed information from sensors to directly perform environment prediction [7–9]. We focus on the latter approach and exploit the rich perception data provided by LiDAR sensors within the autonomous sensor suite. The task is posed as self-supervised sequence-to-sequence learning [10] where a single scenario can be decomposed into an input history sequence and a target prediction sequence. For the environment representation, we use a discrete map in the form of an occupancy grid [11] due to its robustness to partial environment observability [2]. This approach facilitates the use of occupancy state estimation under uncertainty, modeled using either Bayesian methods [11] or Dempster-Shafer Theory (DST) [12], to update our belief about the surroundings.

Prior work in occupancy grid prediction often uses modified Convolutional Long Short Term Memory (ConvLSTM) frameworks [13], tackling occupancy grid prediction onboard both fixed [14] and moving [2, 7] platforms. These architectures are capable of capturing the dynamics of the environment, but they often suffer from mode-averaging and limited long-term dependencies between sequence elements [15]. Both issues lead to significant blurriness of the predicted occupancy grid and the gradual disappearance of moving obstacles, which is a critical aspect of environment prediction [2, 15].

Our method extends the approach for occupancy grid prediction defined by Itkina et al. [2] with *attention* [16–19] in order to improve the long-term dependencies captured by the prediction model. Inspired by the work of Bahdanau et al. [16] and Bello et al. [19], we propose *attention*-based extensions to the ConvLSTM architecture that reduce the prediction blurriness and obstacle disappearance in longer time horizon predictions. Our approach focuses on the fusion of convolution and attention in visual prediction tasks, which requires attending jointly to both feature (what is present in the image), 2D spatial (where the object is in the image) and temporal (when the object is present in the sequence) subspaces. The key contributions in this work are as follows:

- We develop the Temporal Attention Augmented Convolution (TAAConv) operator that enables spatiotemporal attention over a sequence of frames.
- We introduce the Temporal Attention Augmented ConvLSTM (TAAConvLSTM) and the Self-Attention Augmented ConvLSTM (SAAConvLSTM) architectures which encourage long-range dependencies between hidden representations and improve the quality of the predictions for sequence-to-sequence environment prediction tasks.
- We apply the proposed mechanisms to local occupancy grid prediction for a moving ego-vehicle, and demonstrate superior performance compared to other state-of-the-art architectures, such as PredNet [20] and PredRNN++ [21].

We evaluate the proposed mechanisms on two real-world datasets: the KITTI Dataset [22] and the Waymo Open Dataset [23]. We show that our architectures reduce the blurriness and moving obstacle disappearance within the generated predictions.

2 Related Work

Attention: The *attention* mechanism originated in the natural language processing field to create long-term dependencies between different parts of a sentence. Bahdanau et al. [16] showed that extending the conventional recurrent neural network (RNN) encoder-decoder architecture for transduction tasks with attention encourages long-term dependencies between different hidden representations at different sequence locations. Vaswani et al. [17] maintained the encoder-decoder approach but replaced the RNN model with a *Transformer* consisting of a *multi-head self-attention* mechanism. Several works have extended attention with convolution for the purposes of modeling sentence pairs [24], relation classification Wang et al. [25], and re-identification Xu et al. [26]. These approaches do not attend jointly to both feature and 2D spatial subspaces and, therefore, are not directly applicable in visual prediction tasks. Parmar et al. [18] applied attention as a stand-alone vision operator by computing attention over local regions within an image. However, the lack of hardware-accelerated operations generally limits its application. Bello et al. [19] improved efficiency by reformulating self-attention for the purpose of augmenting the convolution operation over images. In this paper, we build on the approach of Bello et al. [19] for the task of occupancy grid prediction.

Video Prediction: Srivastava et al. [27] proposed a sequence-to-sequence LSTM approach to video frame prediction by forming predictions in the representation space of a video sequence. Xingjian et al. [13] extended the LSTM model to capture spatial correlations by adding a convolution operator, thus forming the ConvLSTM. Finn et al. [28] addressed the multimodality of the prediction task by considering an action-conditioned video prediction model. Wang et al. [21] introduced the PredRNN++ architecture, which augments a ConvLSTM with *zigzag* connections and increased recurrence depth (casual ConvLSTM) to model complex short-term dynamics. Lotter et al. [20] proposed a Predictive Coding Network (PredNet), where the error signal between the prediction and the observation is propagated laterally and vertically within the recurrent architecture. The aforementioned approaches focus on deterministic predictive models. A separate category of work tackles stochastic modelling [29, 30], which is beyond the scope of this paper. In this work, we apply video prediction techniques to occupancy grid prediction due to clear parallels between both tasks.

Occupancy Grid Prediction: Various adaptations of the RNN architecture with convolutions are commonly used for occupancy grid prediction tasks. Dequaire et al. [7] proposed a *DeepTracking* approach where an RNN with a Spatial Transformer was used for binary occupancy grid prediction. Schreiber et al. [14] tested a ConvLSTM to predict the occupancy grids for a stationary ego-vehicle in urban settings, such as intersections. Mohajerin and Rohani [31] employed a difference learning

approach assuming a high refresh rate of the LiDAR sensor and high map similarity between frames. Itkina et al. [2] repurposed the PredNet architecture [20] for ego-centric occupancy grid prediction. This approach captured the relative dynamics of static and moving objects well but experienced significant blurring and the gradual disappearance of obstacles. In this paper, we formulate a novel attention-augmented ConvLSTM mechanism and validate it as part of PredNet [20].

3 Background

3.1 Convolutional Long Short-Term Memory (ConvLSTM)

A *ConvLSTM* is an RNN architecture that models spatiotemporal correlations in a sequence. A single ConvLSTM unit comprises of the following elements: a *memory cell* \mathcal{C}_t accumulates information, an *input gate* i_t controls whether to include new information in the memory cell, a *forget gate* f_t maintains the flow of information from the previous time step, and an *output gate* o_t controls the information flow from the memory cell \mathcal{C}_t to the *hidden representation* \mathcal{H}_t . For an input $X \in \mathbb{R}^{H \times W \times F_{in}}$, the ConvLSTM equations are denoted below, where ‘ $*$ ’ is the convolution operator and ‘ \circ ’ is the Hadamard product [13]:

$$\begin{aligned} i_t &= \sigma(W_{xi} * \mathcal{X}_t + W_{hi} * \mathcal{H}_{t-1} + W_{ci} \circ \mathcal{C}_{t-1} + b_i) \\ f_t &= \sigma(W_{xf} * \mathcal{X}_t + W_{hf} * \mathcal{H}_{t-1} + W_{cf} \circ \mathcal{C}_{t-1} + b_f) \\ \mathcal{C}_t &= f_t \circ \mathcal{C}_{t-1} + i_t \circ \tanh(W_{xc} * \mathcal{X}_t + W_{hc} * \mathcal{H}_{t-1} + b_c) \\ o_t &= \sigma(W_{xo} * \mathcal{X}_t + W_{ho} * \mathcal{H}_{t-1} + W_{co} \circ \mathcal{C}_t + b_o) \\ \mathcal{H}_t &= o_t \circ \tanh(\mathcal{C}_t). \end{aligned} \quad (1)$$

$\mathcal{H} \in \mathbb{R}^{d \times H \times W}$ is the hidden representation. $W_{x*}, W_{h*} \in \mathbb{R}^{F_{in} \times k \times k \times d}$ and $W_{c*}, b_* \in \mathbb{R}^{d \times H \times W}$ denote the weights and biases of the architecture, where k is the convolution kernel size.

3.2 Attention Augmented Convolution (AAConv)

Vaswani et al. [17] introduced the self-attention mechanism to model sequential dependencies between elements in a position agnostic manner which Bello et al. [19] applied to visual tasks. For a flattened image $X \in \mathbb{R}^{HW \times F_{in}}$, they defined a *query*: $Q = XW_q$, a *key*: $K = XW_k$, and a *value*: $V = XW_v$, where $W_q, W_k \in \mathbb{R}^{F_{in} \times d_k^h}$, and $W_v \in \mathbb{R}^{F_{in} \times d_v^h}$ are learned projection matrices that map the input to different representation subspaces. Attention then selects or *attends* to the subset of information encoded in the value V . The selection of information is determined by the softmax of the dot product between query Q , and key K . As the query Q , key K , and value V all derive from the original input X , the mechanism dynamically regulates the flow of information that depends on the provided input X rather than the learned masks. Bello et al. [19] formulated attention for visual tasks with a learned positional encoding $S_{H,W}^{rel}$. Single-head attention is evaluated as follows:

$$A_h(Q, K, V)_{ij} = \text{softmax} \left(\frac{q_{i,*} K^T + (S_{H,W}^{rel})_{i,*}}{\sqrt{d_k^h}} \right) v_{*,j}. \quad (2)$$

Multi-head attention concatenates the outputs A_h from different heads h , each with independent projection matrices W_q, W_k and W_v , and fuses them using the learned matrix $W^o \in \mathbb{R}^{d_v \times d_v}$,

$$MHA(Q, K, V) = [A_1, \dots, A_h] W^o. \quad (3)$$

The motivation for multi-head attention is to enable attention in different representational subspaces which prevents the averaging effects present in single-head attention [17]. The output is reshaped into a tensor $H \times W \times d_v$ and concatenated with the output of a convolution creating an Attention Augmented Convolution [19], as follows,

$$AAConv(X) = [Conv(X), MHA(XW_q, XW_k, XW_v)]. \quad (4)$$

4 Methodology

Prior work on ConvLSTM-based prediction frameworks has fundamentally suffered from the gradual and consistent disappearance of moving agents within the predictions, making it unsuitable for

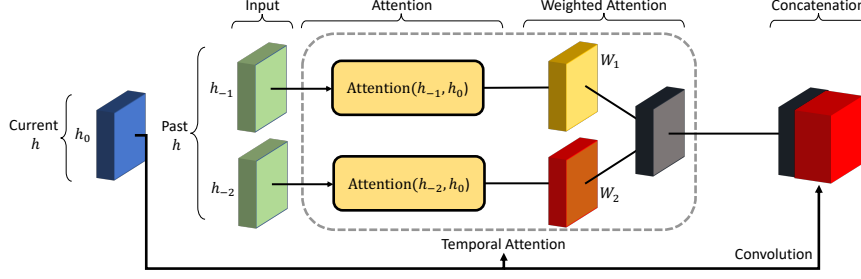


Figure 1: The illustration shows a Temporal Attention Augmented Convolution (TAACConv) with a single head ($N_h = 1$) and $H_a = 2$ attention horizon.

long-horizon prediction and safety-critical applications (See Appendix A). We hypothesize that this phenomenon is caused by the incomplete hidden representation within the ConvLSTM mechanism, which gradually loses the fine-grained detail of dynamic objects. Inspired by the work of Bello et al. [19] and Bahdanau et al. [16], we introduce Temporal Attention Augmented Convolution (TAACConv), which uses attention to draw visual dependencies between different frames. This operator is applied to the state-to-state transitions within the ConvLSTM, forming a Temporal Attention Augmented ConvLSTM (TAACConvLSTM). We posit that this mechanism reduces the loss of information that occurs in the hidden representation over time. Additionally, we propose a Self-Attention Augmented ConvLSTM (SAACConvLSTM), which applies the Self-Attention Augmented Convolution operator to the input-to-state transitions of the ConvLSTM. We postulate that the self-attention extension enforces a more accurate hidden representation resulting in higher quality prediction.

4.1 Environment Prediction Task

We pose the environment prediction task as self-supervised sequence-to-sequence learning consisting of a history input sequence and a prediction output sequence. Given the history, our framework models how the environment evolves over time. As the environment representation, we use belief mass occupancy grids generated using Dempster-Shafer Theory (DST), following prior work [2]. A detailed overview of this approach to occupancy estimation is presented in Appendix B. We define the belief mass occupancy grid $X_k \in \mathbb{R}^{2 \times H \times W}$, which denotes the DST belief mass representation of the environment at time step k . Let us denote the past N frames as $X_{k-N:k}$, which are sequentially provided to our architecture in order to build an internal, dynamic representation of the scene. After the N th frame, the model predicts the future P frames, where P is the prediction horizon. At each future time step $k + \tau$, the prediction $X_{k+\tau}$ recursively serves as input at the next time step $k + \tau + 1$ until time step $k + P$ is reached. Our objective is to predict $X_{k+1:k+P}$.

4.2 Temporal Attention Augmented Convolution (TAACConv)

We formulate an extension to the attention for visual tasks defined by Bello et al. [19] to enable spatiotemporal attention over a sequence of frames. Our approach is presented in Fig. 1. We hypothesize that our attention module will learn to *attend* to the essential moving and static objects in the frame, and recover missing details by drawing direct dependencies between the current and the past H_a frames, where H_a is the attention horizon.

Based on the current input X_t and the past input $X_{t-\tau}$, a new query Q_t , key $K_{t-\tau}$, and value $V_{t-\tau}$ are computed following the attention for visual tasks approach defined in Section 3.2. Attention is then determined for each $(X_{t-\tau}, X_t)$ pair, where $\tau \in 1 : H_a$. Multi-head temporal attention for visual tasks is defined as follows:

$$MHTA(X_t, X_{t-H_a:t-1}) = \sum_{\tau=t-H_a}^{t-1} W_\tau MHA(X_t W_q, X_{t-\tau} W_k, X_{t-\tau} W_v). \quad (5)$$

The output is reshaped into a tensor $H \times W \times d_v$ and concatenated with the output of a convolutional layer:

$$TAACConv(X_t, X_{t-H_a:t-1}) = [Conv(X_t), MHTA(X_t, X_{t-H_a:t-1})]. \quad (6)$$

This method extends the attention for visual tasks [19] to capture long range visual dependencies between the different elements of a sequence.

4.3 Temporal Attention and Self-Attention Augmented ConvLSTM

The prediction quality of a ConvLSTM significantly deteriorates with longer prediction horizons, resulting in substantial blurriness and moving object disappearance [20, 21]. In this work, we formulate two extensions to the ConvLSTM mechanism to address these issues, *Temporal Attention Augmented ConvLSTM (TAAConvLSTM)* and *Self-Attention Augmented ConvLSTM (SAACConvLSTM)*.

Temporal Attention Augmented ConvLSTM (TAAConvLSTM): This approach is motivated by the assumption that the previous hidden representations $\mathcal{H}_{t-1-H_a:t-1}$ contain a more complete encoding of the moving object of interest than the most recent representation \mathcal{H}_{t-1} . We use the TAAConv operation defined in Section 4.2 between \mathcal{H}_{t-1} and $\mathcal{H}_{t-1-H_a:t-1}$ to recover detailed dynamic object predictions, and, as a result, reduce predicted object vanishing. This operator replaces the convolutional operators responsible for state-to-state transitions in the ConvLSTM (Eq. (1)):

$$\begin{aligned} i_t &= \sigma(W_{xi} * \mathcal{X}_t + TAAConv(\mathcal{H}_{t-1}, \mathcal{H}_{t-1-H_a:t-1}) + W_{ci} \circ \mathcal{C}_{t-1} + b_i) \\ f_t &= \sigma(W_{xf} * \mathcal{X}_t + TAAConv(\mathcal{H}_{t-1}, \mathcal{H}_{t-1-H_a:t-1}) + W_{cf} \circ \mathcal{C}_{t-1} + b_f) \\ \mathcal{C}_t &= f_t \circ \mathcal{C}_{t-1} + i_t \circ \tanh(W_{xc} * \mathcal{X}_t + TAAConv(\mathcal{H}_{t-1}, \mathcal{H}_{t-1-H_a:t-1}) + b_c) \\ o_t &= \sigma(W_{xo} * \mathcal{X}_t + TAAConv(\mathcal{H}_{t-1}, \mathcal{H}_{t-1-H_a:t-1}) + W_{co} \circ \mathcal{C}_t + b_o) \\ \mathcal{H}_t &= o_t \circ \tanh(\mathcal{C}_t). \end{aligned} \quad (7)$$

Self-Attention Augmented ConvLSTM (SAACConvLSTM): An alternative approach to mitigating object vanishing is to signalize which elements of the received \mathcal{X}_t to preserve with the self-attention mechanism. We apply the self-attention augmented convolution (Eq. (3)) to the input-to-state transitions of the ConvLSTM (Eq. (1)). The self-attention mechanism allows for selective and dynamic regulation of incoming information to the hidden representation of the ConvLSTM resulting in the improved flow of information. The SSAConvLSTM is formulated as follows:

$$\begin{aligned} i_t &= \sigma(AAConv(\mathcal{X}_t) + W_{hi} * \mathcal{H}_{t-1} + W_{ci} \circ \mathcal{C}_{t-1} + b_i) \\ f_t &= \sigma(AAConv(\mathcal{X}_t) + W_{hf} * \mathcal{H}_{t-1} + W_{cf} \circ \mathcal{C}_{t-1} + b_f) \\ \mathcal{C}_t &= f_t \circ \mathcal{C}_{t-1} + i_t \circ \tanh(AAConv(\mathcal{X}_t) + W_{hc} * \mathcal{H}_{t-1} + b_c) \\ o_t &= \sigma(AAConv(\mathcal{X}_t) + W_{ho} * \mathcal{H}_{t-1} + W_{co} \circ \mathcal{C}_t + b_o) \\ \mathcal{H}_t &= o_t \circ \tanh(\mathcal{C}_t). \end{aligned} \quad (8)$$

5 Experiments

We validate our proposed operators on the real-world KITTI [22] and Waymo [23] datasets. In all experiments, the attention mechanism is implemented as part of the Predictive Coding Network (PredNet) [20], where we replace the ConvLSTM in the top layers with our Attention Augmented ConvLSTM mechanisms. We chose the PredNet architecture for direct comparison with prior environment prediction work [2]. The positional information in the attention calculation is encoded using the relative learned positional encoding defined by Bello et al. [19]. We demonstrate that the TAAConvLSTM and SAACConvLSTM mechanisms significantly reduce the vanishing of moving objects and outperform the baselines including PredNet [20] and PredRNN++ [21]. The TAAConvLSTM is further examined in an ablation study where we investigate how each head of the temporal attention in the proposed TAAConv mechanism affects the prediction.

Experimental Setup: We investigate the capability of our proposed method to make effective long-term predictions and compare it with other state-of-the-art sequence-to-sequence video prediction architectures on the KITTI dataset [22] and Waymo dataset [23]. In all experiments, we follow the procedure defined by Itkina et al. [2], where we provide 5 past DST occupancy grids (0.5 s) sequentially as input and attempt to make predictions for 15 future frames accounting for 1.5 s into the future. We consider occupancy grids of dimension $H \times W = 128 \times 128$, corresponding to $42.7 \times 42.7 \text{ m}^2$. All our models were trained using the PyTorch [32] library with the ADAM [33] optimizer. Models were optimized for 200 epochs with 500 samples per epoch on an Nvidia RTX 2080Ti. We used the training procedure for multiple time step predictions defined by Lotter et al.

[20] that optimizes the $L1$ loss. All baselines were trained on their original implementations. Further experimental details are available in Appendix C.

Evaluation Metrics: We validate our results using traditional metrics for prediction, such as Mean Square Error (MSE). However, evaluating the environment prediction task is challenging due to its multimodal output. Unobserved latent variables, such as intent, influence human decisions resulting in a multimodal future. Hence, we also consider the Image Similarity (IS) metric (See Appendix D) [34]. Contrary to the MSE metric, it successfully captures the variability in object positions between two frames, i.e. ground truth and our prediction, within the calculation of the score.

5.1 KITTI Dataset

We investigate the influence of the attention horizon H_a and the number of heads N_h on our prediction performance. We consider a four-layer PredNet architecture with TAAConvLSTM and SAAConvLSTM implemented in the top one and two layers respectively. Fig. 2 compares the predictions for 2.5 s from PredNet with TAAConvLSTM and SAAConvLSTM. Both our methods demonstrate a significant reduction in the vanishing of moving objects and result in more accurate occlusion propagation. Table 1 reports the quantitative metrics for several hyperparameter choices for the attention horizon H_a and the number of heads N_h . An increase in the attention horizon and the number of heads within the TAAConvLSTM reduces the blurriness and disappearance of objects until reaching diminishing returns at $H_a = 4$ and $N_h = 4$. The SAAConvLSTM more accurately models the ego-vehicle interaction with the environment (Fig. 2 Right). The best performing network uses $N_h = 4$ heads. However, the reduction in dynamic objects disappearance is less pronounced resulting in a higher IS score but lower MSE score than the TAAConvLSTM.

We compare the performance of our mechanisms on the KITTI dataset to that of other state-of-the-art sequence-to-sequence prediction architectures, specifically PredNet [20], and PredRNN++ [21]. Our models outperform the baselines both qualitatively (see Fig. 2) and quantitatively (see Table 4).

Table 1: Hyperparameter selection on the KITTI Dataset (lower is better for all metrics).

H_a	N_h	IS	MSE ($\times 10^{-2}$)
2	4	7.40 ± 0.07	3.74 ± 0.0013
6	4	7.00 ± 0.07	3.77 ± 0.0013
4	2	7.61 ± 0.07	3.92 ± 0.0013
4	4	6.91 ± 0.06	3.62 ± 0.0012
4	6	7.41 ± 0.07	3.82 ± 0.0013
4	8	7.02 ± 0.06	3.80 ± 0.0013

N_h	IS	MSE ($\times 10^{-2}$)
2	7.32 ± 0.06	3.67 ± 0.0012
4	7.38 ± 0.07	3.57 ± 0.0012
6	7.32 ± 0.07	3.68 ± 0.0012

Table 4: Comparison on the KITTI Dataset (lower is better for all metrics).

Model	Parameters (M)	IS	MSE ($\times 10^{-2}$)
PredNet Lotter et al. [20]	6.9	7.68 ± 0.07	3.63 ± 0.0012
PredRNN++ Wang et al. [21]	7.2	8.86 ± 0.08	3.39 ± 0.0009
PredNet with TAAConvLSTM (ours)	7.2	6.91 ± 0.06	3.62 ± 0.0012
PredNet with SAAConvLSTM (ours)	6.7	7.38 ± 0.06	3.57 ± 0.0012

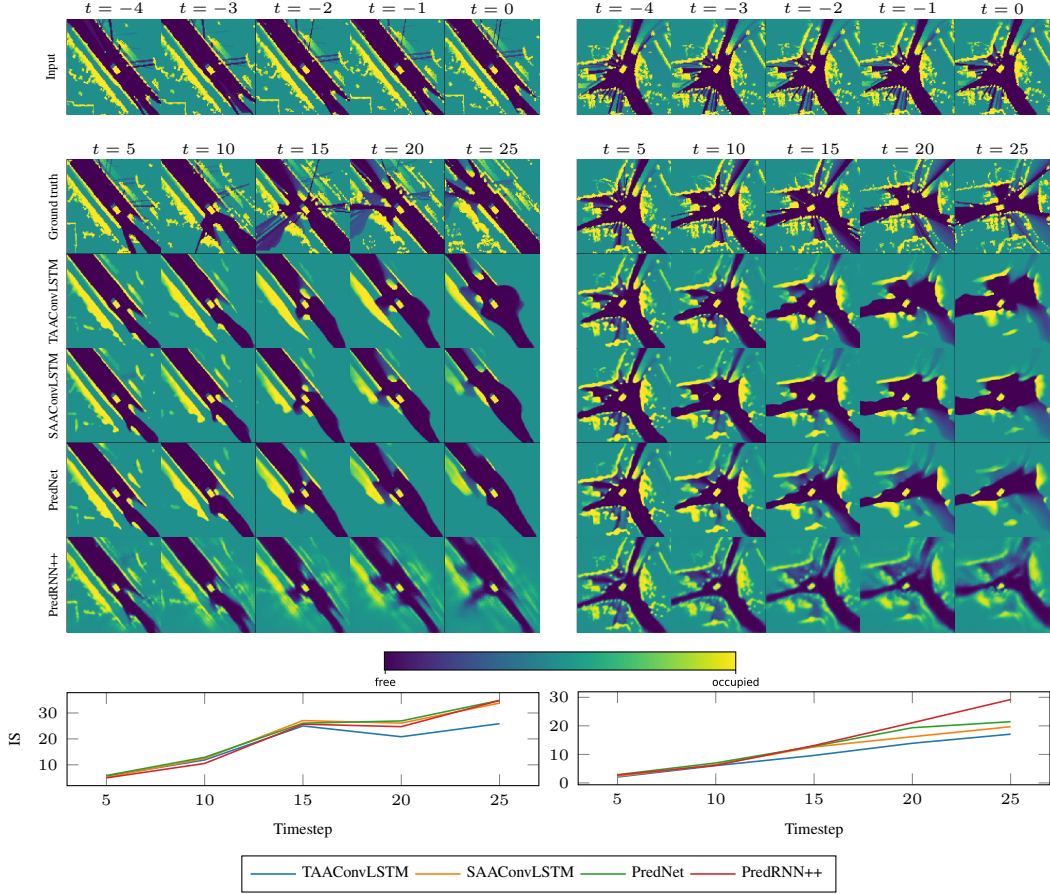


Figure 2: Example 2.5 s predictions on the KITTI dataset and the associated ground truth. Left: The ego-vehicle passes an oncoming vehicle which is preserved in the prediction made by our methods, unlike PredNet. Right: The ego-vehicle makes a turn at an intersection. Our methods maintain the presence of the vehicle adjacent to the ego-vehicle and better represent the intersection. Bottom: Visualization of the IS score per prediction frame (the lower is better) per each of the scenario visualized above.

5.2 Waymo Open Dataset

We further validate our models on the much larger Waymo Open Dataset [23] and compare its performance to the aforementioned baselines. Fig. 3 depicts two example scenarios with interactions at or close to an intersection. In both cases, TAAConvLSTM and SAAConvLSTM outperform visually the PredNet and PredRNN++ baselines. We compare the models quantitatively in Table 5. We observe that SAAConvLSTM underperforms numerically even though qualitatively it performs well. TAAConvLSTM has a superior IS score but is outperformed by the PredRNN++ on the MSE metric due to the significant blurriness of the PredRNN++ predictions, as further discussed in Section 6.

Table 5: Comparison on the Waymo Open Dataset (lower is better for all metrics).

Model	Parameters (M)	IS	MSE ($\times 10^{-3}$)
PredNet Lotter et al. [20]	6.9	3.56 ± 0.04	2.34 ± 0.0063
PredRNN++ Wang et al. [21]	7.2	4.68 ± 0.05	2.25 ± 0.0052
PredNet with TAAConvLSTM (ours)	7.2	3.51 ± 0.04	2.33 ± 0.0063
PredNet with SAAConvLSTM (ours)	6.7	3.64 ± 0.04	2.39 ± 0.0095

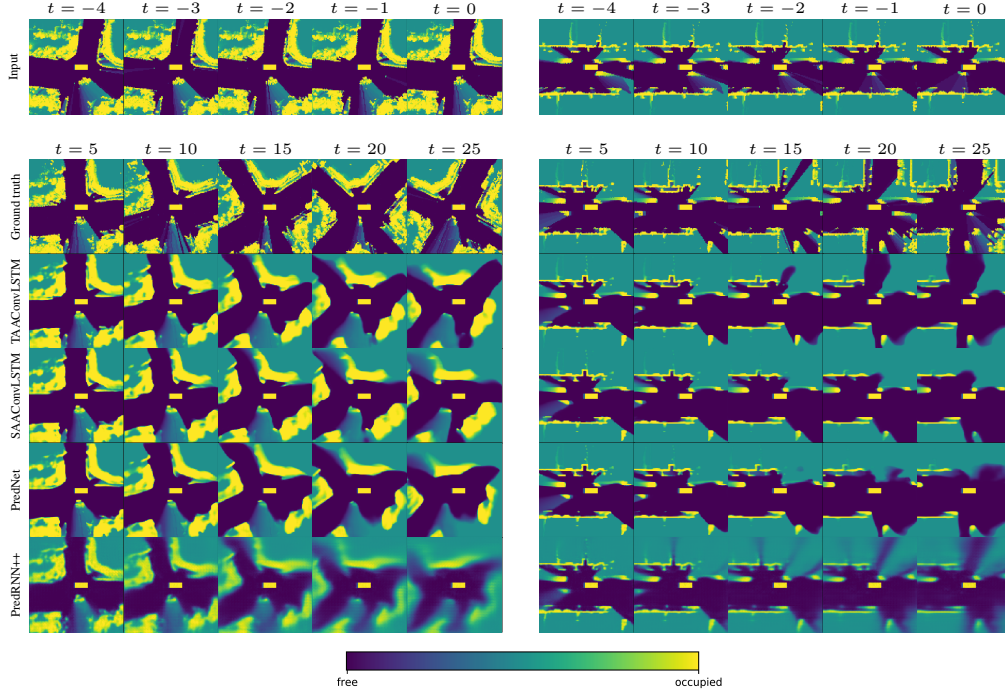


Figure 3: Example 2.5 s predictions on the Waymo dataset and the associated ground truth. Left: The ego-vehicle makes a turn at an intersection. Right: The ego-vehicle approaches an intersection. In both cases, our approaches maintain the presence of the other vehicle at the intersection, in contrast to the baseline predictions. TAAConvLSTM also better captures the static environment rotation and translation.

5.3 Ablation Study

We validate our proposed TAAConv mechanism and investigate how each attention head affects the generated predictions as part of the proposed TAAConvLSTM. We use a smaller variant of our architecture, 3-layer PredNet with TAAConvLSTM at the top layer and 3 attention heads to better understand the workings of our proposed approach. To evaluate how each head contributes to the prediction, we zero out each head’s output one at a time in the attention mechanism and perform the prediction as usual. As shown in Fig. 4, multi-head temporal attention distinctly distributes tasks between each head. Removal of each of the three heads results in: 1) loss of the static environment structure, 2) loss of moving objects, 3) translation offset of the moving objects resulting in a delayed prediction. We hypothesize that the third head learned the motion of the moving objects. Thus, the proposed mechanism plays an important role in our modified PredNet architecture and emphasizes the multimodal capabilities of the attention mechanism.

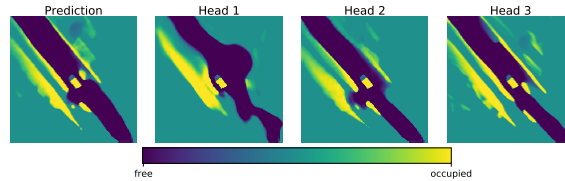


Figure 4: We conduct an ablation study to attempt to understand the proposed attention mechanism better. From left to right: the full prediction, prediction with the first head removed, second head removed, and third head removed, respectively.

6 Discussion and Future Work

Our experiments show that the addition of Temporal Attention and Self-Attention mechanisms to the ConvLSTM reduces the vanishing of moving objects and increases the overall prediction quality of the model. TAACConv enriches the hidden representation of the ConvLSTM and learns to maintain objects’ shapes during motion (Fig. 2 Left). TAACConvLSTM also excels at the relative static environment rotation and static environment inference. It captures correctly the intersection rotation during the ego-vehicle turn (Fig. 3 Left) and infers that there is an incoming intersection (Fig. 3 Right). We hypothesize that the mechanism either encountered similar intersections during training, or learned to infer the semantic layout of the map based on the motion of the other traffic participants. SAACConvLSTM applies the self-attention mechanism to increase the effectiveness of the input-to-state transitions of the ConvLSTM. It maintains higher overall prediction quality with a smaller number of parameters than all other approaches considered.

Both experiments in Section 5.1 and Section 5.2 highlight the challenges of evaluating environment prediction. There is a trade-off between the IS and MSE metrics, which is often present in prediction tasks due to the multimodal characteristics of the problem. The ConvLSTM used in vanilla PredNet tends to blur and remove moving objects from the predictions leading to the lowest MSE for a task with multiple possible futures. This is also visible in the PredRNN++’s predictions. It strategically blurs out the dynamic part of the scene, thus reducing the MSE. Maintaining the dynamic objects in the prediction often results in lower IS and higher MSE. The multi-head temporal and self-attention implemented as part of TAACConvLSTM and SAACConvLSTM facilitate reasoning over multiple representational subspaces and ultimately lead to more detailed predictions with reduced vanishing.

Even though the application of attention in this work is motivated by dynamic object disappearance, our proposed approach appears to learn to *attend* to the static parts of the environment as well as the dynamic objects. The Waymo dataset consists of a considerably larger number of scenarios, the majority of which contain agents with smaller relative velocities with the respect to the ego-vehicle than those in the KITTI dataset. This data imbalance results in a reduced quantitative improvement on the Waymo dataset, but our proposed mechanisms continue to demonstrate qualitatively superior predictions.

There are several further extensions which could be explored for future work. The occupancy grid representation can be augmented with semantic map priors. We can infuse prior information into the attention operator directly to enforce its interpretability. Additionally, positional-encodings for the attention can be tailored to the problem specific task, e.g. exploiting the Inertial Measurement Unit (IMU) in the autonomous driving setting.

Acknowledgments

The authors would like to acknowledge this project being made possible by the funding from the Ford-Stanford Alliance. We thank Ransalu Senanayake for the valuable feedback and Mery Toyungyernsub for help with data processing.

References

- [1] C. Liu, S. Lee, S. Varnhagen, and H. E. Tseng. Path planning for autonomous vehicles using model predictive control. In *Intelligent Vehicles Symposium (IV)*, pages 174–179. IEEE, 2017.
- [2] M. Itkina, K. Driggs-Campbell, and M. J. Kochenderfer. Dynamic environment prediction in urban scenes using recurrent representation learning. In *International Conference on Intelligent Transportation Systems (ITSC)*, pages 2052–2059. IEEE, 2019.
- [3] A. Petrovskaya and S. Thrun. Model based vehicle detection and tracking for autonomous urban driving. *Autonomous Robots*, 26(2-3):123–139, 2009.
- [4] D. Ferguson, M. Darms, C. Urmson, and S. Kolski. Detection, prediction, and avoidance of dynamic obstacles in urban environments. In *Intelligent Vehicles Symposium (IV)*, pages 1149–1154. IEEE, 2008.
- [5] D. I. Ferguson and D. A. Dolgov. Modifying behavior of autonomous vehicle based on predicted behavior of other vehicles, June 4 2013. US Patent 8,457,827.

- [6] Y. Kuwata, J. Teo, S. Karaman, G. Fiore, E. Frazzoli, and J. How. Motion planning in complex environments using closed-loop prediction. In *AIAA Guidance, Navigation, and Control Conference (GNC)*, page 7166, 2008.
- [7] J. Dequaire, D. Rao, P. Ondruska, D. Wang, and I. Posner. Deep tracking on the move: Learning to track the world from a moving vehicle using recurrent neural networks. *arXiv preprint arXiv:1609.09365*, 2016.
- [8] C. C. Chang and K.-T. Song. Environment prediction for a mobile robot in a dynamic environment. *Transactions on Robotics and Automation*, 13(6):862–872, 1997.
- [9] S. Hoermann, M. Bach, and K. Dietmayer. Dynamic occupancy grid prediction for urban autonomous driving: A deep learning approach with fully automatic labeling. In *International Conference on Robotics and Automation (ICRA)*, pages 2056–2063. IEEE, 2018.
- [10] I. Sutskever, O. Vinyals, and Q. V. Le. Sequence to sequence learning with neural networks. In *Advances in Neural Information Processing Systems (NeurIPS)*, pages 3104–3112, 2014.
- [11] A. Elfes. Using occupancy grids for mobile robot perception and navigation. *Computer*, 22(6):46–57, 1989.
- [12] J. Gordon and E. H. Shortliffe. The dempster-shafer theory of evidence. *Rule-Based Expert Systems: The MYCIN Experiments of the Stanford Heuristic Programming Project*, 3:832–838, 1984.
- [13] S. Xingjian, Z. Chen, H. Wang, D.-Y. Yeung, W.-K. Wong, and W.-c. Woo. Convolutional lstm network: A machine learning approach for precipitation nowcasting. In *Advances in Neural Information Processing Systems (NeurIPS)*, pages 802–810, 2015.
- [14] M. Schreiber, S. Hoermann, and K. Dietmayer. Long-term occupancy grid prediction using recurrent neural networks. In *International Conference on Robotics and Automation (ICRA)*, pages 9299–9305. IEEE, 2019.
- [15] C. Tang and R. R. Salakhutdinov. Multiple futures prediction. In *Advances in Neural Information Processing Systems (NeurIPS)*, pages 15398–15408, 2019.
- [16] D. Bahdanau, K. Cho, and Y. Bengio. Neural machine translation by jointly learning to align and translate. In *International Conference on Learning Representations (ICLR)*, 2015.
- [17] A. Vaswani, N. Shazeer, N. Parmar, J. Uszkoreit, L. Jones, A. N. Gomez, L. Kaiser, and I. Polosukhin. Attention is all you need. In *Advances in Neural Information Processing Systems (NeurIPS)*, pages 5998–6008, 2017.
- [18] N. Parmar, P. Ramachandran, A. Vaswani, I. Bello, A. Levskaya, and J. Shlens. Stand-alone self-attention in vision models. In *Advances in Neural Information Processing Systems (NeurIPS)*, pages 68–80, 2019.
- [19] I. Bello, B. Zoph, A. Vaswani, J. Shlens, and Q. V. Le. Attention augmented convolutional networks. In *International Conference on Computer Vision (ICCV)*, pages 3286–3295. IEEE, 2019.
- [20] W. Lotter, G. Kreiman, and D. Cox. Deep predictive coding networks for video prediction and unsupervised learning. In *International Conference on Learning Representations (ICLR)*, 2017.
- [21] Y. Wang, Z. Gao, M. Long, J. Wang, and P. S. Yu. PredRNN++: Towards a resolution of the deep-in-time dilemma in spatiotemporal predictive learning. In *International Conference on Machine Learning (ICML)*, pages 5123–5132, 2018.
- [22] A. Geiger, P. Lenz, C. Stiller, and R. Urtasun. Vision meets robotics: The KITTI dataset. *International Journal of Robotics Research*, 2013.

- [23] P. Sun, H. Kretzschmar, X. Dotiwalla, A. Chouard, V. Patnaik, P. Tsui, J. Guo, Y. Zhou, Y. Chai, B. Caine, et al. Scalability in perception for autonomous driving: Waymo open dataset. In *Computer Society Conference on Computer Vision and Pattern Recognition (CVPR)*, pages 2446–2454. IEEE, 2020.
- [24] W. Yin, H. Schütze, B. Xiang, and B. Zhou. ABCNN: Attention-based convolutional neural network for modeling sentence pairs. *Transactions of the Association for Computational Linguistics*, 4:259–272, 2016.
- [25] L. Wang, Z. Cao, G. De Melo, and Z. Liu. Relation classification via multi-level attention CNNs. In *54th Annual Meeting of the Association for Computational Linguistics (Volume 1: Long Papers)*, pages 1298–1307, 2016.
- [26] S. Xu, Y. Cheng, K. Gu, Y. Yang, S. Chang, and P. Zhou. Jointly attentive spatial-temporal pooling networks for video-based person re-identification. In *International Conference on Computer Vision (ICCV)*, pages 4733–4742. IEEE, 2017.
- [27] N. Srivastava, E. Mansimov, and R. Salakhudinov. Unsupervised learning of video representations using lstms. In *International Conference on Machine Learning (ICML)*, pages 843–852, 2015.
- [28] C. Finn, I. Goodfellow, and S. Levine. Unsupervised learning for physical interaction through video prediction. In *Advances in Neural Information Processing Systems (NeurIPS)*, pages 64–72, 2016.
- [29] A. X. Lee, R. Zhang, F. Ebert, P. Abbeel, C. Finn, and S. Levine. Stochastic adversarial video prediction. *arXiv preprint arXiv:1804.01523*, 2018.
- [30] M. Kumar, M. Babaeizadeh, D. Erhan, C. Finn, S. Levine, L. Dinh, and D. Kingma. VideoFlow: A conditional flow-based model for stochastic video generation. In *International Conference on Learning Representations (ICLR)*, 2020.
- [31] N. Mohajerin and M. Rohani. Multi-step prediction of occupancy grid maps with recurrent neural networks. In *Computer Society Conference on Computer Vision and Pattern Recognition (CVPR)*, pages 10600–10608. 2019, 2019.
- [32] A. Paszke, S. Gross, F. Massa, A. Lerer, J. Bradbury, G. Chanan, T. Killeen, Z. Lin, N. Gimelshein, L. Antiga, et al. Pytorch: An imperative style, high-performance deep learning library. In *Advances in Neural Information Processing Systems (NeurIPS)*, pages 8026–8037, 2019.
- [33] D. P. Kingma and J. Ba. Adam: A method for stochastic optimization. In *International Conference on Learning Representations (ICLR)*, 2014.
- [34] A. Birk and S. Carpin. Merging occupancy grid maps from multiple robots. *Proceedings of the IEEE*, 94(7):1384–1397, 2006.
- [35] D. Nuss, S. Reuter, M. Thom, T. Yuan, G. Krehl, M. Maile, A. Gern, and K. Dietmayer. A random finite set approach for dynamic occupancy grid maps with real-time application. *International Journal of Robotics Research*, 37(8):841–866, 2018.

A Example Visualization of Moving Object Vanishing in the Baseline Framework

Figure 5 shows an example of a moving object vanishing in the prediction of the PredNet [20] baseline. The gradual vanishing results in the complete disappearance of the moving object (yellow vehicle in Fig. 5).

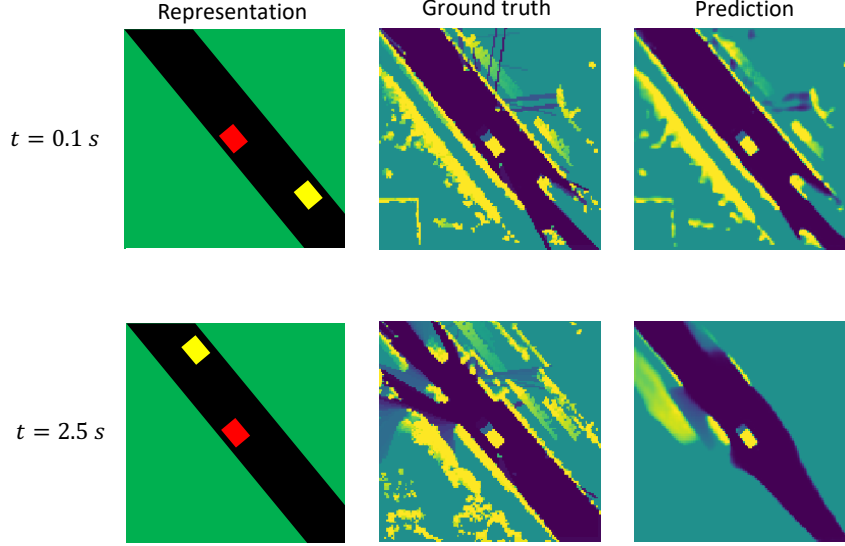


Figure 5: Moving object vanishing. From the left: schematic world representation for illustration, ground truth occupancy grid, and predicted occupancy grid (baseline PredNet). Top row: prediction 0.1 s in to the future. Bottom row: 2.5 s in to the future. Labels used in the world representation: ego-vehicle (red), other moving vehicle (yellow), road (black), and static environment (green).

B Occupancy Grid Generation

This section describes the procedure for generating the occupancy grid to form the input and target data for the proposed network. The occupancy grid is generated according to the procedure used by Itkina et al. [2]. To perform the occupancy grid update, two types of methods can be considered: Bayesian methods and Dempster-Shafer Theory (DST) [35]. DST is a decision-making strategy that provides evidential updates in support of or against a set of the hypotheses given the evidence. It can distinguish between uncertainty and lack of knowledge [12]. The additional information provided by DST methods enriches our understanding of the surroundings and improves the environment prediction models [2].

Our occupancy grid is updated following the Dempster-Shafer Theory (DST) approach described by Nuss et al. [35] which considers the set of possible *events* defined in a *frame of discernment* Ω . For the occupancy grid scenario, the events are free space F and occupied space O , i.e. $\Omega = F, O$. The possible set of hypotheses is defined as the power set of Ω which is $2^\Omega = \{\emptyset, \{F\}, \{O\}, \{F, O\}\}$, where \emptyset denotes the empty set. Each hypothesis has a corresponding belief mass. The sum of belief masses over the hypothesis set is equal to 1. The proposition \emptyset can be pruned from our set because a cell cannot be neither occupied and unoccupied. The initial condition for the belief masses assigns one to the $\{F, O\}$ set representing the unknown state of the cell. Therefore, the mass over all other hypotheses is zero because there is no evidence stating that the cell is occupied or free until sensor measurements are received.

Subsequently, the DST update rule defined in Eq. (9) is used with every new measurement to update the previous mass m_{k-1}^c in cell c at time step k with new measurement $m_{k,z}^c$ [35]:

$$\begin{aligned} m_k^c(A) &= m_{k-1}^c \oplus m_{k,z}^c(A) \\ &:= \frac{\sum_{X \cap Y = A} m_{k-1}^c(X) m_{k,z}^c(Y)}{1 - \sum_{X \cap Y = \emptyset} m_{k-1}^c(X) m_{k,z}^c(Y)} \\ &\quad \forall A, X, Y \in \{\{F\}, \{O\}, \{F, O\}\}. \end{aligned} \quad (9)$$

Before each measurement, we perform information aging to the prior masses:

$$\begin{aligned} m_{k,\alpha}^c(\{O\}) &= \min(\alpha \cdot m_k^c(\{O\}), 1) \\ m_{k,\alpha}^c(\{F\}) &= \min(\alpha \cdot m_k^c(\{F\}), 1) \\ m_{k,\alpha}^c(\{F, O\}) &= 1 - m_{k,\alpha}^c(\{O\}) - m_{k,\alpha}^c(\{F\}). \end{aligned} \quad (10)$$

An estimate of conventional occupancy grid probabilities are acquired using the concept of pignistic probability:

$$betP(B) = \sum_{A \in 2^\Omega} m(A) \cdot \frac{|B \cap A|}{|A|} \quad (11)$$

C Architectures

In the following section, we outline the architectures considered in this paper, which are PredNet [20], PredNet with TAAConvLSTM (ours), PredNet with SAAConvLSTM (ours), and Pre-dRNN++ [21]. All architectures follow a sequence-to-sequence model where we provide a number of past frames and predict the future frames. For each architecture, we provide a short overview of the framework and hyperparameters.

C.1 Predictive Coding Network (PredNet)

Lotter et al. [20] developed a *Predictive Coding Network* (PredNet) architecture which serves as a baseline for this paper. A single *prediction cell* alongside its entire architecture are presented in Figs. 6 and 7, respectively. The single PredNet prediction cell consists of the following elements: an input convolutional layer (A_l), a recurrent representation layer (R_l), a prediction layer (\hat{A}_l), and an error representation (E_l). The relationship governing the transitions between elements are shown in the following equation:

$$\begin{aligned} A_l^t &= \begin{cases} x_t, & \text{if } l = 0 \\ \text{MaxPool}(\text{ReLU}(\text{Conv}(E_{l-1}^t))), & l > 0 \end{cases} \\ \hat{A}_l^t &= \text{ReLU}(\text{Conv}(R_l^t)) \\ E_l^t &= [\text{ReLU}(A_l^t - \hat{A}_l^t); \text{ReLU}(\hat{A}_l^t - A_l^t)] \\ R_l^t &= \text{ConvLSTM}(E_l^{t-1}, R_l^{t-1}, \text{Upsample}(R_{l+1}^t)) \end{aligned} \quad (12)$$

Such prediction cells can be stacked to form larger and more capable recurrent networks. In this paper, we consider a 4-layer setup which consists of 4 PredNet prediction cells. More details are presented in Table 6.

Table 6: PredNet Architecture Details.

Hyperparameter	Value
Number of layers/cells	4
Number of hidden units per layer	2, 48, 96, 192
Filter size per layer	3, 3, 3, 3
Number of parameters	6 912 766

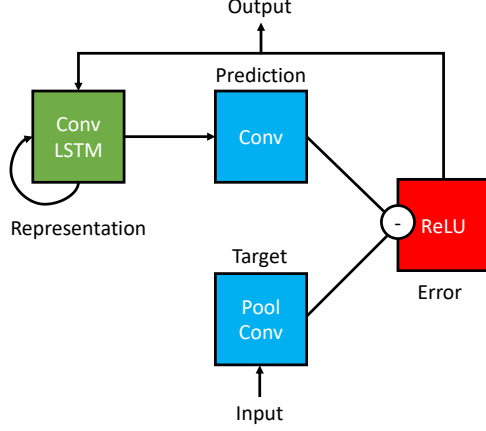


Figure 6: Prediction cell for the Predictive Coding Network (PredNet) created by Lotter et al. [20].

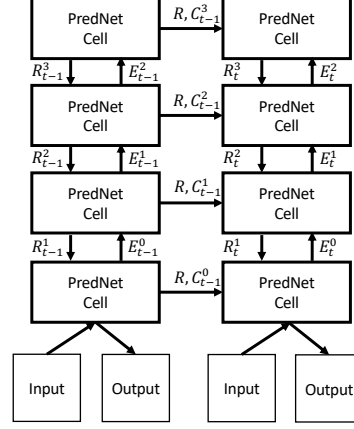


Figure 7: The architecture with 4 stacked PredNet prediction cells used in this paper.

C.2 Predictive Coding Network with TAAConvLSTM

In the first proposed approach, we replace the ConvLSTM in the top (4th) PredNet prediction cell with the TAAConvLSTM mechanism. The relationships for the PredNet prediction cell with TAAConvLSTM are as follows:

$$\begin{aligned}
 A_l^t &= \begin{cases} x_t, & \text{if } l = 0 \\ \text{MaxPool}(\text{ReLU}(\text{Conv}(E_{l-1}^t))), & l > 0 \end{cases} \\
 \hat{A}_l^t &= \text{ReLU}(\text{Conv}(R_l^t)) \\
 E_l^t &= [\text{ReLU}(A_l^t - \hat{A}_l^t); \text{ReLU}(\hat{A}_l^t - A_l^t)] \\
 R_l^t &= \text{TAAConvLSTM}(E_l^{t-1}, R_l^{t-1}, \text{Upsample}(R_{l+1}^t), R_l^{t-1-H_a:t-1})
 \end{aligned} \tag{13}$$

In our formulation, we define the attention horizon as the H_a most recent past representations $R^{t-1-H_a:t-1}$. However, we saw an improvement when selecting the H_a past frames uniformly covering a period of 1 s, instead of using the most recent H_a frames covering a period of $H_a \times \Delta_t$ (0.4 s). This change resulted in a further reduction of moving object vanishing from the predictions. We believe that this choice is more representative of the motion of the agents present in the input scene. Equivalently to attention for visual tasks defined by Bello et al. [19], a memory cost of $O((HW)^2 N_h H_a)$ should be noted. The overview of the framework is Table 7.

Table 7: PredNet with TAAConvLSTM Architecture Details.

Hyperparameter	Value
Number of layers/cells	4
Layers with ConvLSTM	1, 2, 3
Number of hidden units per layer	2, 48, 96, 192
Filter size per layer	3, 3, 3, 3
Layers with TAAConvLSTM	4
Number of heads in TAAConvLSTM	4
Attention horizon	4
Attention hidden units d_k, d_h	$0.25 \times$ hidden units at layer
Numbers of parameters	7 222 094

C.3 Predictive Coding Network with SAACovLSTM

In our second approach, we applied Attention Augmented Convolution introduced by Bello et al. [19] to the input-to-state transitions of the ConvLSTM, formulating SAACovLSTM. The equations for the mechanisms are:

$$\begin{aligned}
A_l^t &= \begin{cases} x_t, & \text{if } l = 0 \\ \text{MaxPool}(\text{ReLU}(\text{Conv}(E_{l-1}^t))), & l > 0 \end{cases} \\
\hat{A}_l^t &= \text{ReLU}(\text{Conv}(R_l^t)) \\
E_l^t &= [\text{ReLU}(A_l^t - \hat{A}_l^t); \text{ReLU}(\hat{A}_l^t - A_l^t)] \\
R_l^t &= \text{SAACovLSTM}(E_l^{t-1}, R_l^{t-1}, \text{Upsample}(R_{l+1}^t))
\end{aligned} \tag{14}$$

SAACovLSTM uses a more memory efficient self-attention mechanism ($O((HW)^2 N_h)$). The overview of the architecture is shown in Table 8.

Table 8: PredNet with SAACovLSTM Architecture Details.

Hyperparameter	Value
Number of layers/cells	4
Layers with ConvLSTM	1, 2
Number of hidden units per layer	2, 48, 96, 192
Filter size per layer	3, 3, 3, 3
Layers with SAACovLSTM	3, 4
Number of heads in SAACovLSTM	4
Attention horizon	4
Attention hidden units d_k, d_h	$0.25 \times$ hidden units at layer
Numbers of parameters	6 705 118

C.4 PredRNN++

Wang et al. [21] introduced the PredRNN++ architecture which achieved state-of-the-art results on video prediction tasks. Wang et al. [21] developed the casual LSTM, which increases the recurrence depth between time steps and better captures short-term dynamics between frames. Additionally, the architecture includes a Gradient Highway Unit (GHU) to tackle the vanishing gradients issue. The PredRNN++ architecture is shown in Fig. 8.

The casual LSTM introduces more nonlinear recurrent transitions and dual memory, the temporal memory \mathcal{C}_t^k and spatial memory \mathcal{M}_t^k . The relationships governing the casual LSTM are as follows:

$$\begin{aligned}
\begin{pmatrix} g_t \\ i_t \\ f_t \end{pmatrix} &= \begin{pmatrix} \tanh \\ \sigma \\ \sigma \end{pmatrix} W_1 * [\mathcal{X}_t, \mathcal{H}_{t-1}^k, \mathcal{C}_{t-1}^k] \\
C_t^k &= f_t \circ C_{t-1}^k + i_t \circ g_t \\
\begin{pmatrix} g'_t \\ i'_t \\ f'_t \end{pmatrix} &= \begin{pmatrix} \tanh \\ \sigma \\ \sigma \end{pmatrix} W_2 * [\mathcal{X}_t, \mathcal{C}_t^k, \mathcal{M}_t^{k-1}] \\
\mathcal{M}_t^k &= f'_t \circ \tanh(W_3 * \mathcal{M}_t^{k-1}) + i'_t \circ g'_t \\
o_t &= \tanh(W_4 * [\mathcal{X}_t, \mathcal{C}_t^k, \mathcal{M}_t^k]) \\
\mathcal{H}_t^k &= o_t \circ \tanh(W_5 * [\mathcal{C}_t^k, \mathcal{M}_t^k])
\end{aligned} \tag{15}$$

where $W_{1:5}$ are the weights for the convolutional layers. The GHU relationships are as follows:

$$\begin{aligned}
\mathcal{P}_t &= \tanh(W_{px} * \mathcal{X}_t + W_{pz} * \mathcal{Z}_{t-1}) \\
\mathcal{S}_t &= \sigma(W_{sx} * \mathcal{X}_t + W_{sz} * \mathcal{Z}_{t-1}) \\
\mathcal{Z}_t &= \mathcal{S}_t \circ \mathcal{P}_t + (1 - \mathcal{S}_t) \circ \mathcal{Z}_{t-1}
\end{aligned} \tag{16}$$

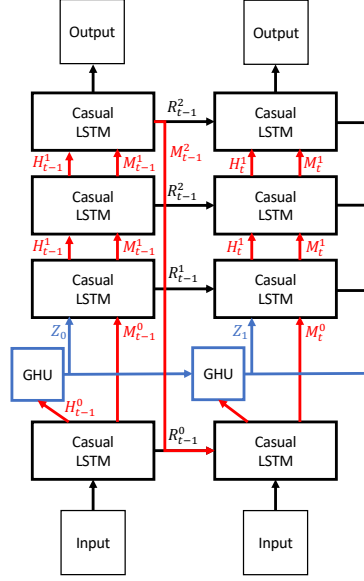


Figure 8: The PredRNN++ setup used in this paper. 4 casual LSTM cells with Gradient Highway Unit (GHU) applied between the first and second layers.

Table 9: PredRNN++ Architecture Details.

PredRNN++	
Number of layers/cells	4
Number of hidden units per layer	64, 64, 64, 64
Filter size per layer	5, 5, 5, 5
Stride	1
Patch Size	4
Numbers of parameters	7 249 344

where W_{**} are the convolutional layer weights, \mathcal{S}_t is a *Switch Gate*, \mathcal{P}_t is the transformed input, and \mathcal{Z}_t is the hidden state. The architecture details used in this paper are presented in Table 9.

D Image Similarity Metric

The Image Similarity (IS) metric, defined by Birk and Carpin [34], determines the picture distance function ψ between two matrices m_1 and m_2 , as follows:

$$\psi(m_1, m_2) = \sum_{c \in \mathcal{C}} d(m_1, m_2, c) + d(m_2, m_1, c) \quad (17)$$

where

$$d(m_1, m_2, c) = \frac{\sum_{m_1[p]=c} \min\{\text{md}(p_1, p_2) | m_2[p_2] = c\}}{\#_c(m_1)} \quad (18)$$

\mathcal{C} is a set of discretized values assumed by m_1 or m_2 which are: occupied, occluded, and free. $m_1[p]$ denotes the value c of map m_1 at position $p = (x, y)$. $\text{md}(p_1, p_2) = |x_1 - x_2| + |y_1 - y_2|$ is the Manhattan distance between points p_1 and p_2 . $\#_c(m_1) = \#\{p_1 | m_1[p_1] = c\}$ is the number of cells in m_1 with value c .

E Additional Results

We report additional plot representing the IS values versus the prediction horizon in Fig. 9. The performance gap between our TAAConvLSTM and the baseline algorithms increases with longer time horizon predictions, demonstrating that our algorithm reduces vanishing, and thus maintains longer-term temporal dependencies.

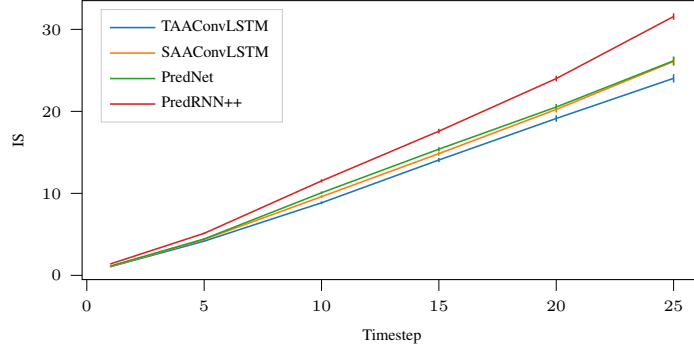


Figure 9: The plot represent IS value versus the prediction horizon for 2.5s prediction horizon. We can observe that the performance gap between TAAConvLSTM and the baselines increases with longer time horizon predictions.